IEEE Access
Multidisciplinary ⋮ Rapid Review ⋮ Open Access Journal

Received 10 August 2022, accepted 1 September 2022, date of publication 12 September 2022, date of current version 19 September 2022.

Digital Object Identifier 10.1109/ACCESS.2022.3206005

RESEARCH ARTICLE

Design of a Harmonic Suppressed Dual-Band Reconfigurable Bandpass Filter for Multistandard GNSS Receivers

XUE MAO [1], WENJIN LIU [2], AND JINGCHANG NAN [1]
[1]School of Electronic and Information Engineering, Liaoning Technical University, Huludao 125105, China
[2]School of Electronic and Information Engineering, Liaoning Technical University, Fuxin 123000, China

Corresponding author: Xue Mao (xywmtmx@163.com)

This work was supported in part by the National Natural Science Foundation of China General Program under Grant 61971210.

ABSTRACT This paper proposes a reconfigurable dual-band bandpass filter with independently tunable center frequencies that is intended to be integrated into reconfigurable multiband global navigation satellite system receivers. The center frequencies can be adjusted within the range of 1160-1280 MHz and 1530-1630 MHz for the two passbands, respectively. To achieve the design goal, the input and output feed lines are shared by a pair of quarter-wave uniform impedance resonators and a stub-loaded stepped impedance resonator with terminal-loaded varactor bias circuits. The electric length of the transmission lines is changed by using bias voltage to control the varactor diodes, thereby changing the operating frequencies of the dual-band filter's two passbands, and the independent reconfigurability of the two passbands is realized. The insertion loss is less than 1.5 dB and the return loss is better than 26 dB in all tuning ranges. The proposed dual-band reconfigurable filter demonstrates the flexibility of controlling the passband independently to be compatible with multistandard signals, which can accommodate the deployment of new GNSS standard specifications.

INDEX TERMS Bandpass filter, dual-band, GNSS receiver, harmonic suppressed, reconfigurable, varactor diode.

I. INTRODUCTION

Geographic positioning and satellite navigation technology have advanced rapidly in recent years, with far-reaching implications for people's daily lives. GNSS (Global Navigation Satellite System) services are now available in a wide range of scenarios, including geolocation, aviation, telecommunications, etc. With the rapid advancement of science and technology, some countries have developed their own navigation systems, such as GPS(Global Positioning System) in the United States, Galileo(Galileo Navigation Satellite System) in Europe, GLONASS(Global Navigation Satellite System) in Russia, and BDS(BeiDou Navigation Satellite System) in China. The field of GNSS research is gaining popularity [1], [2], [3], [4]. The GNSS equipment used should be compatible with multistandard signals to improve positioning accuracy in harsh environments. Furthermore, the devices are expected to be highly integrated with low power consumption. Multi-mode receivers capable of operating across multiple frequency bands are critical for these navigation system devices. Under this development trend, it is necessary to use RF modules that could adjust the central frequency based on the needs, and reconfigurable filters [5], [6], [7], [8], [9], [10], [11] that can tune the frequency mode flexibly will play an important role.

Filters with multiple passbands, such as dual-band bandpass filters(DBBPF), are more advantageous in GNSS applications. Based on waveguide-slot membranes, a waveguide compact filter is proposed in [12]. The designed filter has good passband characteristics in the L1 and L2 bands and is suitable for use in GLONASS/GPS navigation systems. Reference [13] proposes a new type of dual-band filter formed by a closed-loop rectangular ring resonator. The double degenerate modes can be split by using the open-circuit stub as the perturbation element. The two passbands set specially are intended to function in the L1 and L2 bands of GPS.

The associate editor coordinating the review of this manuscript and approving it for publication was Chun-Hsing Li.

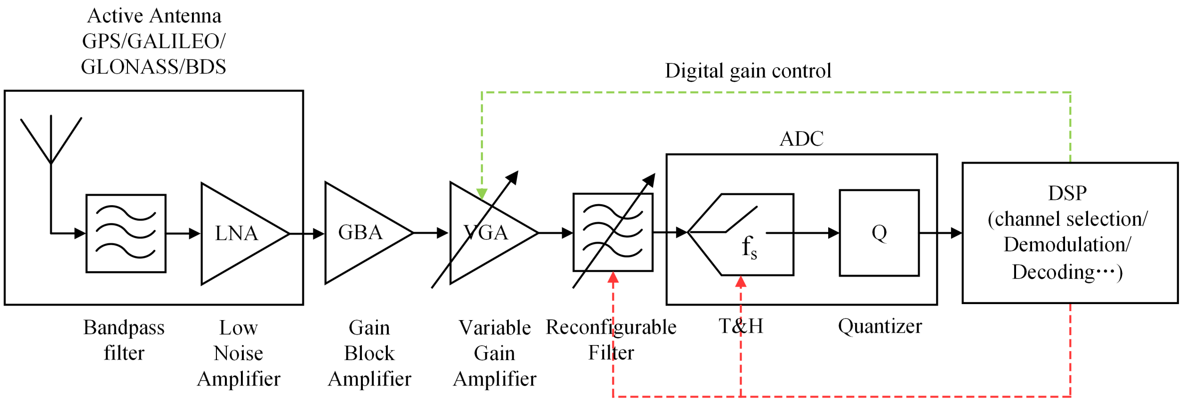

FIGURE 1. **Reconfigurable GNSS subsampling receiver.**

A three-band ultra-compact bandpass filter ground on a dual-mode quarter-wave resonator is designed in [14]. The filter is made up of three quarter-wave resonators that allow each designed passband to be controlled without interfering with each other. This method yields three controllable working bands, which are used in GSM, GPS, and WiFi, respectively. Reference [15] presents a reconfigurable DBBPF with reconfigurable frequency and fixed bandwidth for use as an anti-aliasing filter combined in a reconfigurable sampling GNSS receiver. The designed filter has the capability of independently controlling the center frequencies of two bands using the coupling structure of two open-loop short column-loaded resonators. Reference [16] presents a silicon integrated dual-band filter for GNSS. The filter structure is made up of two orthogonal coupled transverse filtering parts, each of which is composed of a quadrature power coupler in reflection mode. It enables the feedforward signal combination effect between two electrical paths of transmission zeros to obtain the sharp impedance double-band filter response.

This paper emphasizes the design of a reconfigurable DBBPF with independently reconfigurable center frequencies for GNSS applications. The proposed filter implements the two passbands by using a pair of quarter-wave uniform impedance resonators(UIR) and a stub-loaded stepped impedance resonator(SLSIR), respectively, and varactor diodes are loaded to implement the reconfiguration of the center frequency. Furthermore, the input/output feed lines use a source-load coupling structure to increase transmission zeros, and a defective ground structure (DGS) is used to suppress harmonics, further optimizing the transmission characteristics of the proposed filter.

The framework of the study described in the paper is organized as below: Section II introduces the structure of a reconfigurable RF subsampling receiver and deduces the design goal of a reconfigurable filter. The structure and characteristics of this dual-band bandpass filter are then introduced in detail in section III. Section IV then provides the design and implementation of the reconfigurable filter, as well as simulation and measured results. Finally, in section V, the conclusion is given.

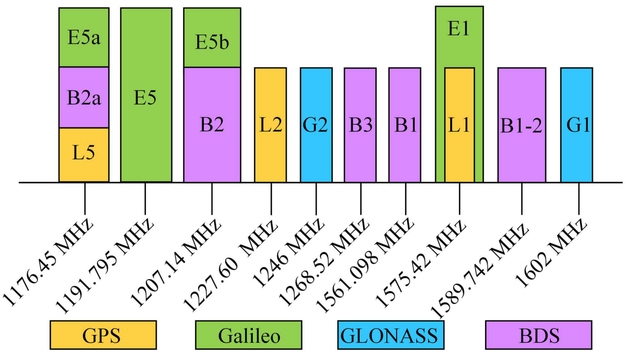

FIGURE 2. **Allocation of GNSS signals.**

II. RECONFIGURABLE SUBSAMPLING RECEIVERS AND FILTER SPECIFICATIONS

Fig.1 depicts the structure of the reconfigurable GNSS subsampling receiver. The expected processing objects are signals from GPS, GLONASS, Galileo, and BDS satellites. The goal of the GNSS receiver is to simultaneously receive and process multiple standard GNSS signals as shown in Fig.2.

The designation of each module is indicated in Fig.1. The reconfigurable subsampling receiver includes an active antenna for capturing all GNSS signals and amplifying them with minimal additional noise. Because the GNSS signal's reception power is quite low, a GBA is placed to boost the signal's level. A VGA is adopted apart from the GBA to control the power level of the ADC input. An ADC composed of a T&H circuit plays the role of subsampling GNSS signals as well as downconverting them to IF in the digital domain. The ADC's sampling frequency must be adjusted to downconvert only available GNSS signals while consuming less power. Finally, DSP is connected for the detection and analysis of GNSS signals. The purpose of this paper is to design a DBBPF with center frequency reconfiguration performance for a reconfigurable GNSS subsampling receiver. This filter's passbands can be applied to the service from GPS, GLONASS, Galileo, and BDS systems.

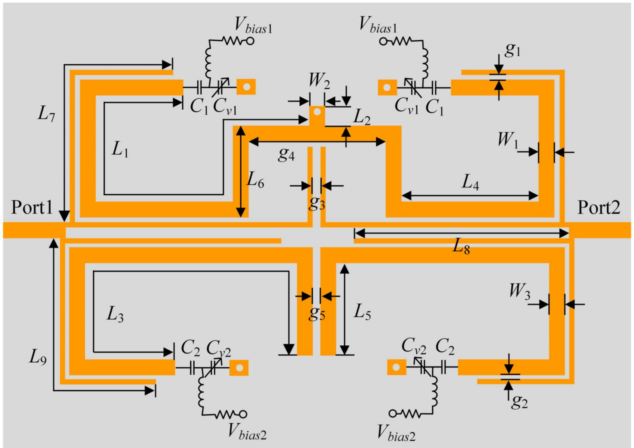

FIGURE 3. Layout of the proposed reconfigurable dual-band filter.

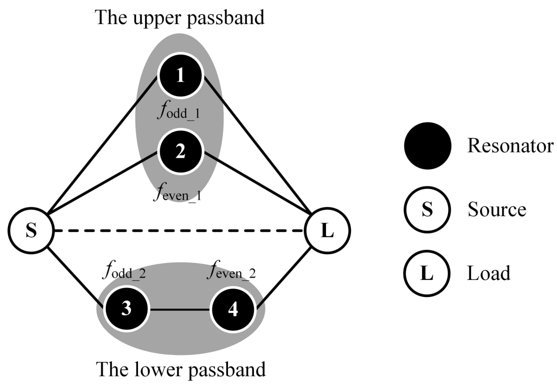

FIGURE 4. Coupling topology of the proposed reconfigurable DBBPF.

III. THEORETICAL FOUNDATION AND DESIGN STRATEGY

The basic structure of this reconfigurable DBBPF is depicted in Fig.3. The major proportion of the resonator is composed of a pair of quarter-wave UIR and a SLSIR, each of which forms a passband. Each resonator is outfitted with varactor diodes, and the resonator's energy is supplied by π-shaped input/output feed lines. The UIR and SLSIR are both folded to use space more efficiently. Fig. 4 shows the corresponding circuit coupling topology. Black nodes 1 and 2 represent SLSIR's odd- and even-modes, while black nodes 3 and 4 represent UIR's odd- and even-modes. The source and load are represented by hollow nodes. The two resonant units operate with common laid I/O feeders. The improved π-shaped I/O feed lines are folded properly and source-load coupling is introduced by using the improved π-shaped I/O feed lines. The two types of resonators are placed on different sides of the feed lines, respectively, minimizing coupling interference between these resonators and allowing for more efficient feeding. The coupling between the two passbands is very weak as a result, and the two passbands can be controlled independently.

A. CHARACTERISTICS OF THE SLSIR

The SLSIR's layout is depicted in Fig.5(a). A short-circuit stub is loaded in the transmission line's center, and two identical varactor diodes are concatenated to the transmission line's end. Each branch's characteristic admittance is denoted by Y, and its length is denoted by L. Since the shape of the SLSIR is left-right symmetrical, the even-odd mode derivation process could be utilized to calculate the resonant frequency in the theoretical derivation. When the odd-mode excitation is exerted on the resonator as represented in Fig.5(a), the symmetrical surface can be regarded as an ideal electric wall, and the circuit with equivalent characteristics of which is depicted in Fig.5(b). The resonator's odd-mode input admittance Y_{ino_1} is given as:

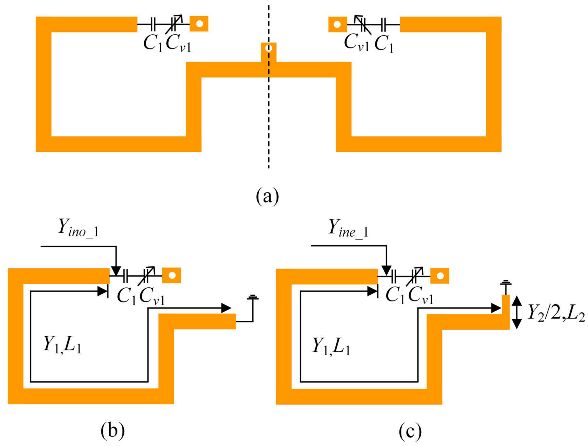

FIGURE 5. (a) Layout of the SLSIR (b) Odd-mode (c) Even-mode.

$$Y_{ino\_1} = j\left(\omega C_{11} - Y_1 \cot\theta_1\right) \tag{1}$$

where $\theta_1 = \beta L_1$ represents the electrical length, β is the phase constant, and C_{11} denotes the total capacitance of the DC blocking capacitor C_1 and the varactor diode C_{v1} wired in series:

$$C_{11} = \frac{C_1 C_{v1}}{C_1 + C_{v1}} \tag{2}$$

According to the resonant condition

$$\mathrm{Im}\left[Y_{ino\_1}\right] = 0 \tag{3}$$

The odd-mode resonant frequency of the SLSIR can be deduced as

$$f_{odd\_1} \times \tan\left(\frac{2\pi\sqrt{\varepsilon_r}L_b f_{odd\_1}}{c}\right) = \frac{Y_b}{2\pi C_{11}} \tag{4}$$

According to (4), changing the state of the varactor causes the variation of odd-mode resonant frequency f_{odd_1}. And f_{odd_1} decreases as the capacitance C_{v1} of the varactor diode increases. Changing the varactor's capacitance C_{v1} is equivalent to changing the physical length L_1 of the microstrip line, achieving the goal of adjusting the odd-mode resonant frequency.

When even-mode excitation is carried out, the symmetric surface can be regarded as an ideal magnetic wall, which is equivalent to an open circuit, as demonstrated in Fig.5(c). The center operating frequency of the multimode resonator can be shifted by affecting varactor diode C_{v1} loaded by the open

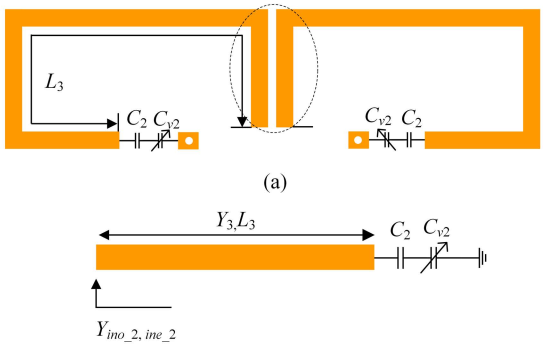

FIGURE 6. **(a) Layout of the UIR (b) Equivalent circuit.**

circuit transmission line. The resonator's even-mode input admittance Y_{ine_1} can be expressed as

$$Y_{ine\_1} = j\left(\omega C_{11} + Y_1 \frac{Y_2/2 \tan\theta_2 + Y_1 \tan\theta_1}{Y_1 - Y_2/2 \tan\theta_2 \tan\theta_1}\right) \tag{5}$$

where $\theta_i = \beta L_i (i = 1, 2)$ represents the electrical length. In order to simplify the calculation, assume that $Y_1 = Y_2/2$. According to the resonant condition

$$\mathrm{Im}\left[Y_{ine\_1}\right] = 0 \tag{6}$$

The even-mode resonant frequency of the SLSIR can be obtained as

$$f_{even\_1} \times \cot\left(\frac{2\pi\sqrt{\varepsilon_r}(L_1 + L_2) f_{even\_1}}{c}\right) = \frac{Y_1}{2\pi C_{11}} \tag{7}$$

According to (7), the even-mode resonant frequency f_{even_1} can be determined by the capacitance of varactor diode C_{v1} loaded at both ends of the transmission line. Changing V_{bias1} can affect C_{v1}, thereby adjusting f_{even_1}. And f_{even_1} decreases as the capacitance of C_{v1} increases in the case where L_2 is very small. Changing C_{v1} can equivalently tune the physical length of the microstrip line, thus altering f_{even_1}.

It can be seen from (4) and (7) that f_{odd_1} and f_{even_1} both change with the capacitance of varactor diode C_{v1}. And since f_{odd_1} and f_{even_1} form a passband together, varactor diode C_{v1} can control the center working frequency of the SLSIR, enabling the upper band to be reconfigurable.

B. CHARACTERISTICS OF THE UIR

Fig.6 depicts the quarter-wave UIR loaded with varactor diodes, which is made up of a couple of uniform impedance transmission lines with the admittance of Y_3 and length of L_3. The open ends of the two transmission lines are coupled together, and the opposite end is loaded with a varactor diode C_{v2}. The resonant unit's input admittance is

$$Y_{ino\_2,ine\_2} = jY_3 \frac{\omega_2 C_{22} + Y_3 \tan\theta_3}{Y_3 - \omega_2 C_{22} \tan\theta_3} \tag{8}$$

where $\theta_3 = \beta L_3$ represents the electrical length, β is the phase constant, and C_{22} denotes the total equivalent capacitance of the DC blocking capacitor C_2 and the varactor diode C_{v2} wired in series:

$$C_{22} = \frac{C_2 C_{v2}}{C_2 + C_{v2}} \tag{9}$$

According to the resonant condition

$$\mathrm{Im}\left[Y_{ino\_2}\right] = \mathrm{Im}\left[Y_{ino\_2}\right] = 0 \tag{10}$$

The resonant frequency of the UIR can be obtained as

$$f_{odd\_2,even\_2} \times \tan\left(\frac{2\pi\sqrt{\varepsilon_r} L_3 f_{odd\_2,even\_2}}{c}\right) = \frac{Y_3}{2\pi C_{22}} \tag{11}$$

It can be derived from (9) and (11) that the center operating frequency of the resonator can be shifted by affecting C_{v2}. The center working frequency of the UIR decreases as the value of C_{v2} increases. Changing the capacitance of the varactor diode C_{v2} is equivalent to altering the physical length L_3 of the microstrip line, thus achieving the purpose of altering the resonant frequency.

Two microstrip lines with the characteristic impedance of 50Ω are used to feed the resonators weakly to reduce the influence of input/output feed lines on the coupling coefficient between resonators to investigate the proposed filter's resonant characteristics. Fig.7 depicts the analog amplitude of the weakly coupled circuit as a function of different varactor capacitances (C_{v1} and C_{v2}). The resonant conditions of the above two modes of upper and lower passbands can be tuned simultaneously when C_{v1} and C_{v2} are adjusted. This feature can be utilized in the design of filters with reconfigurable characteristics of both passbands.

C. COUPLING COEFFICIENTS

To estimate and design the filter's two passbands, the coupling coefficients K_1 and K_2 of the upper and lower passbands can be calculated using the following formula[17]

$$K_{1,2} = \frac{f_{odd}^2 - f_{even}^2}{f_{odd}^2 + f_{even}^2} \tag{12}$$

where f_{odd} and f_{even} are the resonant frequencies of different modes in the upper and lower passbands, respectively. Fig.8 (a) and (b) show the coupling coefficients K_1 and K_2 extracted under various conditions. The length and gap width of the resonator coupling regions are represented by L_6, L_5, G_4, and G_5, respectively. The coupling coefficient K_1 of the upper passband decreases as G_4 or L_6 increases. Similarly, the coupling coefficient K_2 of the lower passband increases with increasing G_5 and decreases with increasing L_5. The values of G_4, G_5, L_5, and L_6 can be determined according to these regulations to meet the requirements of passband bandwidth.

D. EXTERNAL QUALITY FACTORS

The external quality factors Q_{e1} and Q_{e2} of the filter's upper and lower passbands with I/O coupling can be derived as follows:

$$Q_{e1} = \pi f_1 \tau_{S11\_1} \tag{13}$$

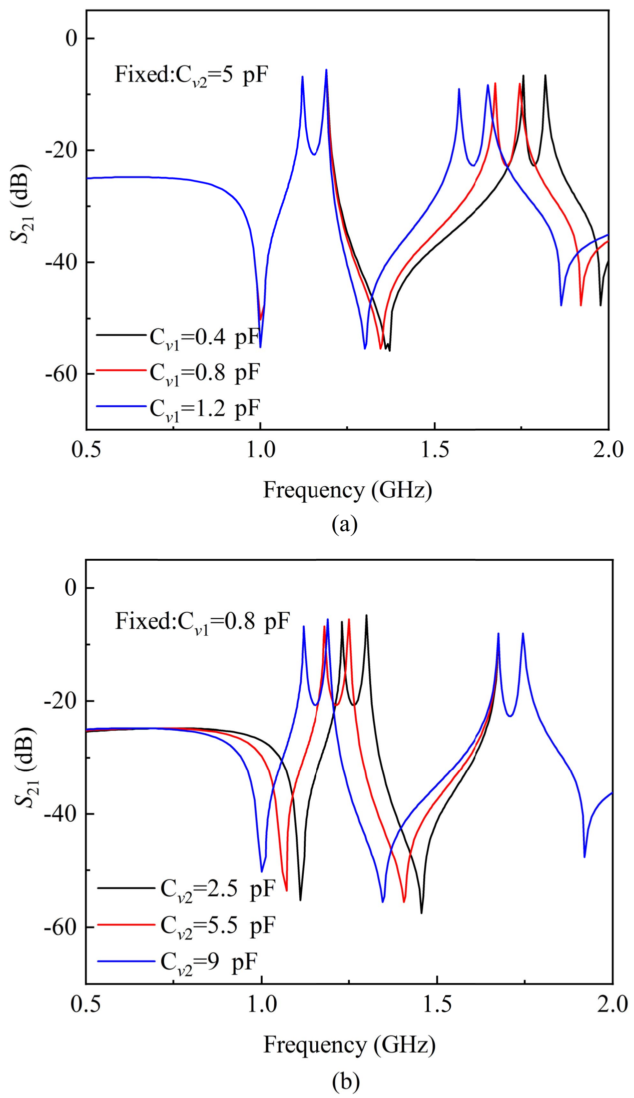

FIGURE 7. **Frequency response under weak coupling (a) The upper band (b) The lower band.**

$$Q_{e2} = \pi f_2 \tau_{S11\_2} \tag{14}$$

where f_1 and f_2 are center frequencies of the upper and lower passbands, and τ_{S11_1} and τ_{S11_2} are the group delays of S_{11} at the passband's center frequencies, respectively. Fig.9 illustrates the extracted Q_{e1} and Q_{e2} for various feeding parameters. The figure shows that as the width of the coupling gap between the resonator and the feeder G_1 and G_2 increases, so do the external quality factors Q_{e1} and Q_{e2}. Furthermore, Q_{e1} and Q_{e2} are inversely proportional to feeding lengths L_7 and L_9, respectively. The above features can be used to estimate the values of the feeding parameters G_1, G_2, L_7, and L_9.

E. DESIGN PROCEDURES

The required independently tunable DBBPF can be designed in the light of the above theoretical analysis, and the detailed design procedures are listed as follows.

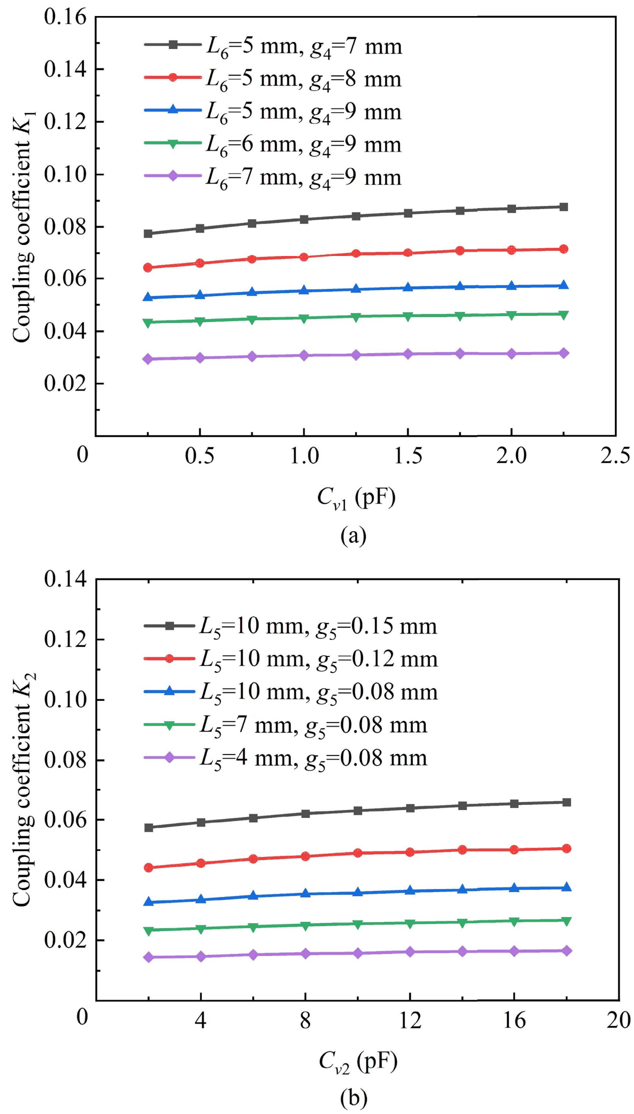

FIGURE 8. **Coupling coefficients (a) The upper band (b) The lower band.**

1) DETERMINE THE DESIRED RECONFIGURABLE DBBPF's EXPECTED PERFORMANCE

- Upper/lower passband center frequency adjustment range: 1.53-1.63/1.16-1.28 GHz;
- 3dB-ABW: 75-95 MHz.

The theoretical $K_{1,2}$ and $Q_{e1,e2}$ can be obtained using these following formulas:

$$K_{1,2} = \frac{ABW_{1,2}}{f_{1,2}\sqrt{g_1 g_2}} \tag{15}$$

$$Q_{e1,e2} = \frac{f_{1,2} g_0 g_1}{ABW_{1,2}} \tag{16}$$

where g_0, g_1, and g_2 are the second-order element values of Chebyshev response low-pass prototype filter with 0.1 dB band ripple, and $g_0 = 0.8430$, $g_1 = 0.6220$, $g_2 = 1.3554$.

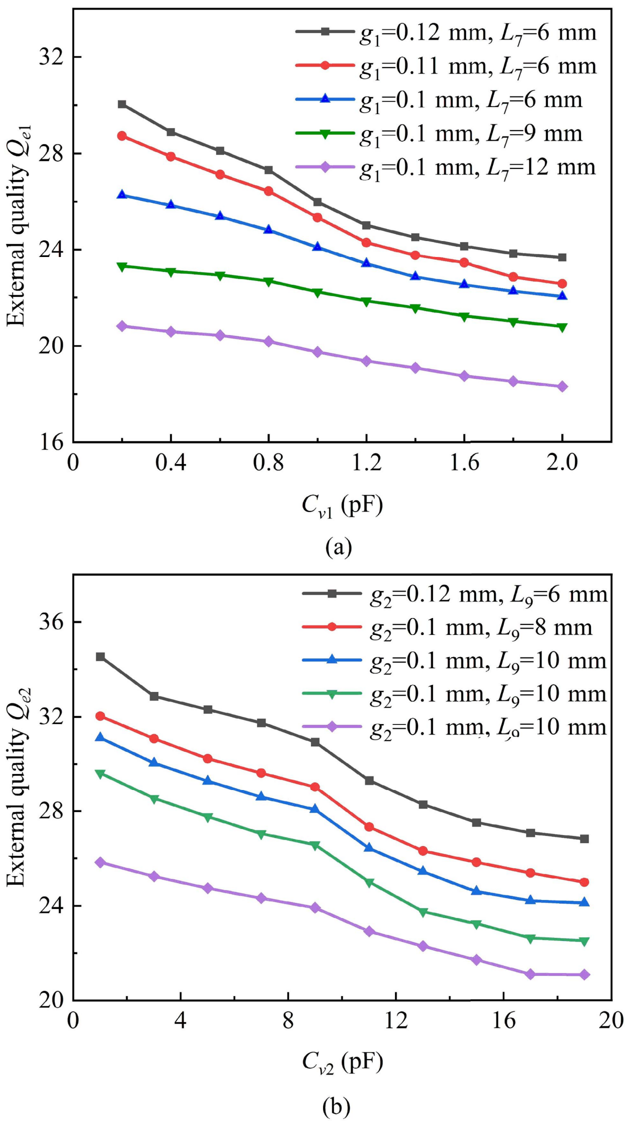

FIGURE 9. External quality factors (a) The upper band (b) The lower band.

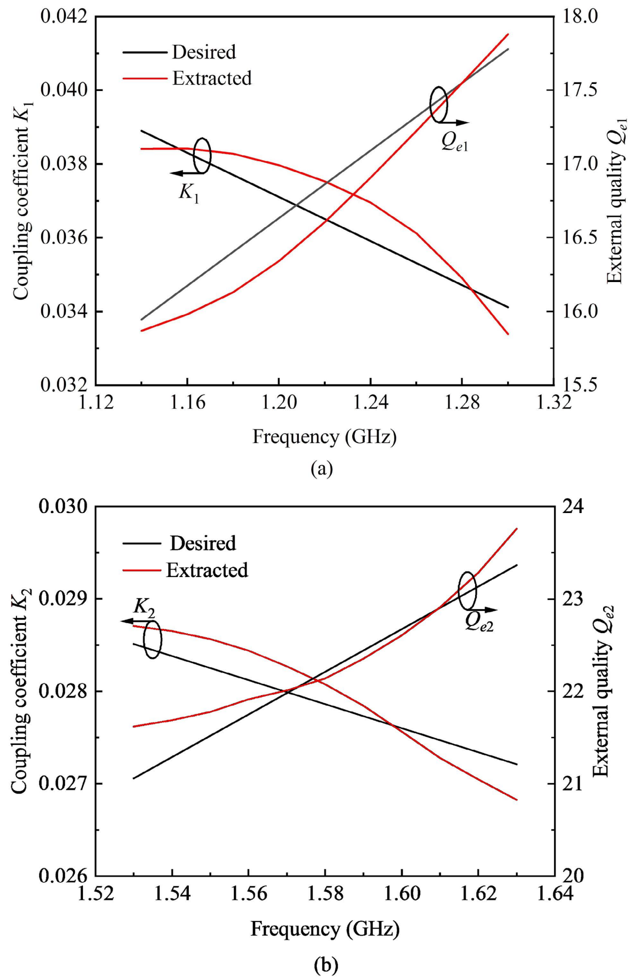

FIGURE 10. Desired and extracted $k_{1,2}$ and $Q_{e1,e2}$ (a) The upper band (b) The lower band.

2) REALIZE THE FREQUENCY TUNING RANGE OF UPPER AND LOWER PASSBAND

The odd- and even-mode resonant frequencies ought to be determined by utilizing (4), (7), and (11), respectively, by selecting the parameters of the structure and the capacitance of the varactor diodes relative to the upper and lower passbands, and identifying the center frequencies of the two passbands.

3) DESIGN COUPLING AND INPUT/OUTPUT STRUCTURES

Following that, the coupling line lengths (L_5 and L_6) and gap widths (g_4 and g_5) are designed based on (12) to meet the frequency response configuration and working bandwidth requirements of the two passbands in (15). Similarly, the relevant feed structure parameters, g_5 and L_7, can be adjusted to satisfy the Q_{e1} and Q_{e2} requirements according to (16). Fig.10 compares the desired $K_{1,2}$ and $Q_{e1,e2}$ with the extracted values closest to the desired $K_{1,2}$ and $Q_{e1,e2}$. In Fig.10, the expected characteristics and actual extracted values of the ideal tunable filter sum are marked with black and red lines, respectively, to facilitate comparison.

4) ADJUST AND OPTIMIZE PARAMETERS

Finally, the joint optimization design is carried out through simulation tools. Circuit parameter estimates from the above steps are plugged into the DBBPF's physical composition in the simulator for simulation of the entire reconfigurable filter circuit, including considerable discontinuity effects, via effects, non-adjacent coupling effects, and lumped element losses, etc. Fine-tune the structural parameters of the filter to better meet the design requirements.

IV. FILTER IMPLEMENTATION AND VERIFICATION

It is discovered that there are harmonics near the upper passband of the designed filter through preliminary simulation. These harmonics will interfere with the filtering effect,

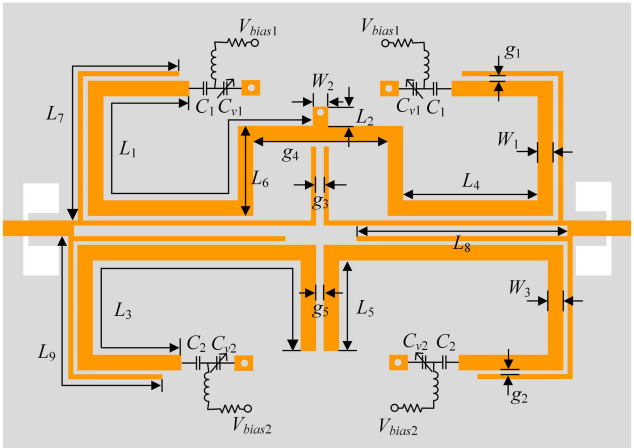

FIGURE 11. Layout of the improved filter.

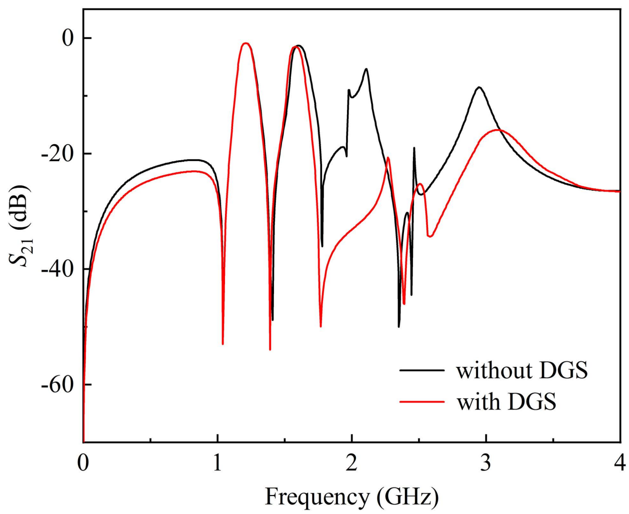

FIGURE 12. Harmonic suppression effect of the improved filter.

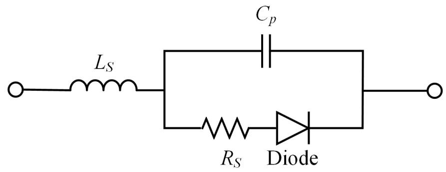

FIGURE 13. SPICE model of the varactor diodes.

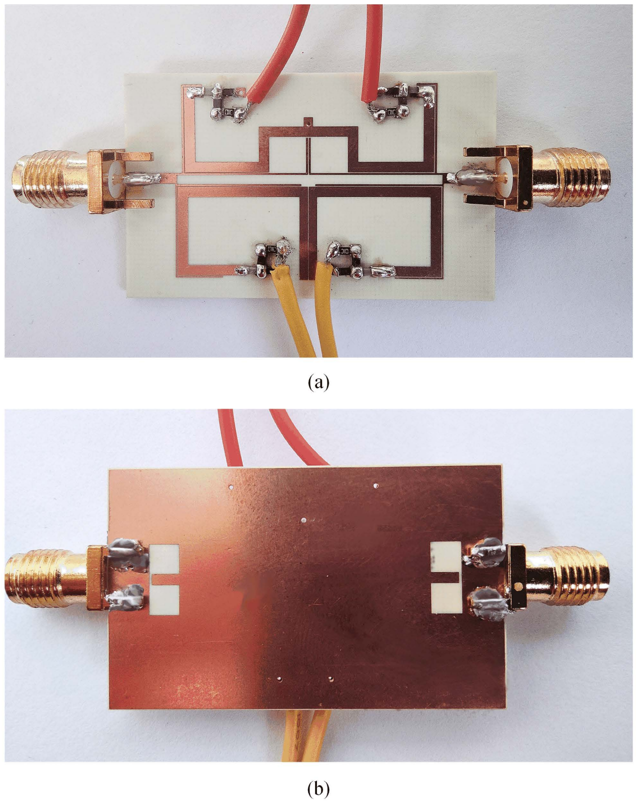

FIGURE 14. Photograph of the fabricated filter (a)Top side (b)Bottom side.

so they must be suppressed for the overall system's performance. The designed filter employs the source-load coupling method to increase transmission zeros and improve filter selectivity, but the passband characteristics require further improvement. The defective ground structure (DGS) is used in this case to further limit the influence of harmonics.

The DGS is realized by introducing additional defects on the backside of the PCB board, which provides band-stop characteristics on a specific resonant band. DGS also enhances the inductance of the transmission lines, allowing transmission lines' slow-wave coefficient to be increased. DGS's bandstop characteristics and slow-wave effects have been used to design a variety of microwave circuits, including filters [18], [19], [20], power splitters [21], [22], antennas [23], [24], [25], [26], etc.

The structure of the harmonic suppression reconfigurable dual-frequency filter with DGS is shown in Fig.11. DGS is used in this structure for inductive coupling at the input/output feeders to suppress filter harmonics. Fig.12 depicts the harmonic suppression characteristic of the proposed filter. It can be seen that the improved filter's stopband characteristic on the outside of the passband is better than 15 dB, demonstrating that this method can achieve harmonic suppression while maintaining passband performance.

Based on the theoretical analysis presented above, a reconfigurable DBBPF is designed and implemented for the multistandard GNSS RF sampling receivers. The electromagnetic (EM) simulation software Ansoft HFSS and Agilent ADS are used to perform field and circuit co-simulation of the designed structure. The proposed filter is constructed on a Rogers RO4003 dielectric substrate with thickness $h = 0.508$ mm and loss tangent $\varepsilon_r = 0.0027$. Two kinds of Skyworks varactors are utilized in the filter: C_{v1} for tuning the upper passband is SMV2019-079LF (with a capacitance value of 0.3-2.22 pF at an applied voltage of 20-0 V) and C_{v2} for tuning the lower passband is SMV1235-079LF (with a capacitance value of 2.38-18.22 pF at an applied voltage of 15-0 V). Fig.13 plots the SPICE model of these varactor

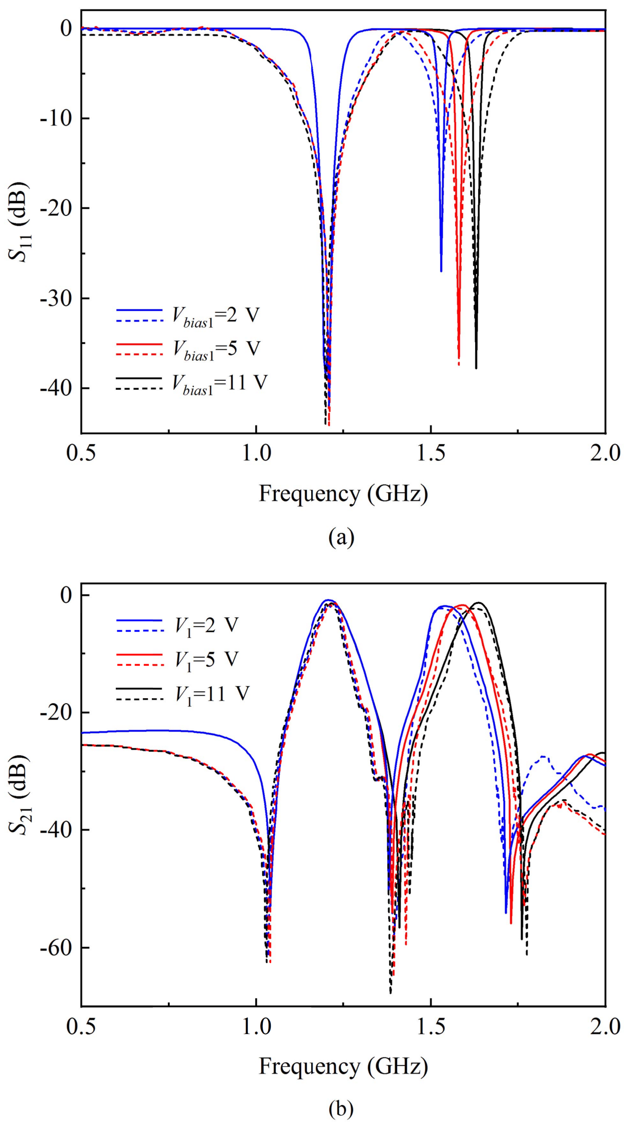

FIGURE 15. Simulated and measured results of the upper passband (a) S_{11} (b) S_{21}.

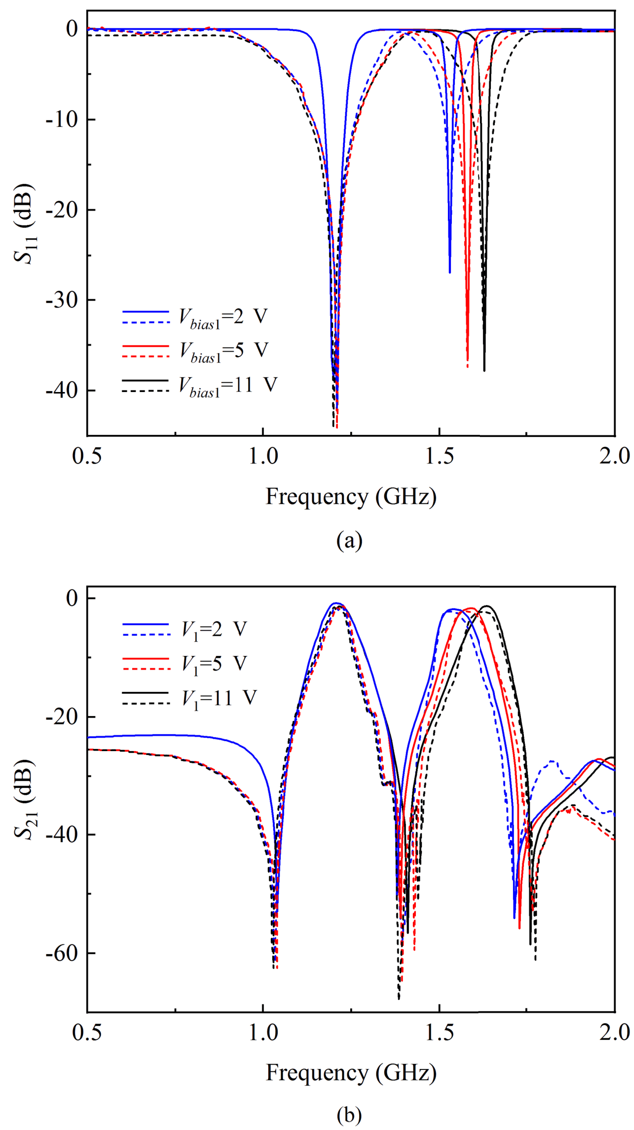

FIGURE 16. Simulated and measured results of the lower passband (a) S_{11} (b) S_{21}.

diodes generated from the manufacturer's datasheets. C_1 and C_2 are 10 pF DC blocking capacitors. A radio frequency choke is formed by connecting a 10 μH inductor and a 10kΩ resistor in series to barred high-frequency signals from entering the DC bias circuit. The overall dimensions of the fabricated filter are 38.5 mm×24.3 mm (i.e., 0.148 λg×0.09 λg, where λg is the wavelength of the filter at the lowest center frequency). Table 1 provides the parameters of the proposed reconfigurable DBBPF's final layout. Fig.14 depicts the photograph of the fabricated filter.

The characteristics achieved by the reconfigurable DBBPF, whose center frequencies of the upper and lower passbands can be adjusted independently, are inferred from Fig.15 and Fig.16. The simulation and test results are represented by solid and dashed lines, respectively. As drawn in Fig.15, the upper center frequency can be tuned in the 1.53-1.63 GHz range with a stationary lower passband, covering the L2/L5 bands of GPS, the G2 band of GLONASS, the E5/E5a/b bands of Galileo, and the B2/B2a bands of BDS. The filter's return loss S_{21} is less than 2.1 dB in this tuning range and its insertion loss S_{11} is better than 26 dB with 3dB-ABW of 85±8 MHz. Fig.16 demonstrates that the lower center frequency can be shifted in the range of 1.15-1.28 GHz when the upper passband is fixed, which is compatible with the L1

TABLE 1. Structural parameters of the DBBPF(mm).

L_1	L_2	L_3	L_4	L_5	L_6
26.025	1	38	8	9	3.8
L_7	L_8	L_9	W_1	W_2	W_3
11.4	13.5	15.1	1.1	1	1.1
g_1	g_2	g_3	g_4	g_5	
0.12	0.14	0.1	8.45	0.15	

TABLE 2. Comparison of filters performance with other references.

Reference	Applications for GNSS	Reconfigurability	Passbands	Center frequency (MHZ)	Insertion loss (dB)	Return loss (dB)	Overal size (mm × mm)
[12]	GLONASS/GPS (L1/L2)	NO	Single-band	1604.5 1249	0.576 1.073	19.3 19.4	50×30 50×30
[13]	GPS (L1/L2)	NO	Dual-band	1220 1570	0.08 0.06	37 30	50.1×42.2
[14]	GPS (L2)	NO	Triple-band	1.57	1.1	15	22×21
[15]	Some mainstream GNSS signals	YES	Dual-band	1191∼1200 1555∼1570	<3.5 <4	>10	84×38
This work	More mainstream GNSS signals	YES	Dual-band	1150∼1280 1530∼1630	<1.5 <2.1	>34 >26	38.5×24.3

band of GPS, G1 band of GLONASS, E1 band of Galileo, and B1/B3 bands of BDS. The filter's return loss S_{21} is less than 1.5 dB in this tuning range and its insertion loss S_{11} is better than 34 dB with 3dB-ABW of 87±7 MHz. The input/output feed lines introduce source-load coupling, so that each passband has a transmission zero on both sides, resulting in good passband selection characteristics. The experimental results meet the expected requirements well and some errors may be attributed to the fabrication tolerances.

Table 2 compares the proposed filter's performance to that of other GNSS-related filters in the literature. The proposed DBBPF can provide tunable characteristics and as a reconfigurable RF filter applied to GNSS, it has relatively good passband characteristics and a considerable frequency domain to cover GNSS signals.

V. CONCLUSION

This paper describes the design of a RF reconfigurable DBBPF for multistandard GNSS receivers. To achieve the desired tuning capability, the proposed filter topology incorporates a pair of UIR and a SLSIR loaded with varactor diodes. A prototype filter is realized in the end, with the working range of both upper and lower passbands covering multiple standard GNSS signals. The experimental results demonstrate that the filter's two passbands have good passband characteristics over the entire frequency range of operation. The proposed reconfigurable DBBPF has satisfactory frequency selectivity and flexible frequency tuning ranges, which can play an effective role in the performance optimization of GNSS receivers.

REFERENCES

[1] K. Cao, L. Wang, B. Li, and H. Ma, "A real-time phase center variation compensation algorithm for the anti-jamming GNSS antennas," *IEEE Access*, vol. 8, pp. 128705–128715, 2020.

[2] J. Lee, J. Han, C.-L. Lo, J. Lee, W. Kim, S. Kim, B. Kang, J. Han, S. Jung, T. Nomiyama, J. Lee, T. B. Cho, and I. Kang, "NB-IoT and GNSS all-in-one system-on-chip integrating RF transceiver, 23-dBm CMOS power amplifier, power management unit, and clock management system for low cost solution," *IEEE J. Solid-State Circuits*, vol. 55, no. 12, pp. 3400–3413, Dec. 2020.

[3] F. Ilyas, S. Irteza, N. Shoaib, and H. M. Cheema, "A frequency agile dual-band GNSS receiver front end with anti-jamming capabilities," in *Proc. Eur. Navigat. Conf. (ENC)*, Nov. 2020, pp. 1–6.

[4] S. Mansoor, N. Shoaib, H. M. Cheema, and A. Shamim, "Single feed dual-band RHCP dielectric resonator antenna for GNSS applications," in *Proc. Int. Appl. Comput. Electromagn. Soc. Symp. (ACES),* Hamilton, ON, Canada, 2021, pp. 1–4.

[5] H. Xu, Y. Wang, F. A. Ghaffar, and L. Roy, "Reconfigurable microwave filters implemented using field programmable microwave substrate," *IEEE Trans. Microw. Theory Techn.*, vol. 69, no. 2, pp. 1344–1354, Feb. 2021.

[6] X. Chen, T. Yang, and P.-L. Chi, "Novel single-ended-to-balanced filter with reconfigurable working modes, frequency, bandwidth, and single/dual-band operations," *IEEE Access*, vol. 9, pp. 14216–14227, 2021.

[7] Z. Wei, T. Yang, P.-L. Chi, X. Zhang, and R. Xu, "A 10.23–15.7-GHz varactor-tuned microstrip bandpass filter with highly flexible reconfigurability," *IEEE Trans. Microw. Theory Techn.*, vol. 69, no. 10, pp. 4499–4509, Oct. 2021.

[8] X.-K. Bi, X. Zhang, S.-W. Wong, S.-H. Guo, and T. Yuan, "Design of notched-wideband bandpass filters with reconfigurable bandwidth based on terminated cross-shaped resonators," *IEEE Access*, vol. 8, pp. 37416–37427, 2020.

[9] D. Psychogiou, "Reconfigurable all-pass-to-bandstop acoustic-wave-lumped-element resonator filters," *IEEE Microw. Wireless Compon. Lett.*, vol. 30, no. 8, pp. 745–748, Aug. 2020.

[10] B. Gowrish and R. R. Mansour, "A novel bandwidth reconfigurable waveguide filter for aerospace applications," *IEEE Microw. Wireless Compon. Lett.*, vol. 30, no. 8, pp. 577–580, Jun. 2020.

[11] S. Yang, W. Li, M. Vaseem, and A. Shamim, "Additively manufactured dual-mode reconfigurable filter employing VO_2-based switches," *IEEE Trans. Compon., Packag., Manuf. Technol.*, vol. 10, no. 10, pp. 1738–1744, Oct. 2020.

[12] D. K. Ogorodnikov, N. F. Kharitonova, Y. A. Litinskaya, and Y. P. Salomatov, "Compact GLONASS band-pass filter based on waveguide with resonance membranes," in *Proc. 15th Int. Sci.-Tech. Conf. Actual Problems Electron. Instrum. Eng. (APEIE)*, Nov. 2021, pp. 264–267.

[13] E. S. Ahmed, "Design of L1/L2 GPS BPF using closed-loop rectangular ring resonator," *IETE J. Res.*, vol. 67, no. 6, pp. 738–743, Jan. 2019.

[14] A. Basit, M. I. Khattak, A. R. Sebak, A. B. Qazi, and A. A. Telba, "Design of a compact microstrip triple independently controlled pass bands filter for GSM, GPS and WiFi applications," *IEEE Access*, vol. 8, pp. 77156–77163, 2020.

[15] R. Barrak, A. Othman, G. I. Abib, M. Müller, M. Mabrouk, and A. Ghazel, "Design of a tunable anti-aliasing filter for multistandard RF subsampling GNSS receivers," *IEEE Trans. Circuits Syst. II, Exp. Briefs*, vol. 66, no. 2, pp. 207–211, Feb. 2019.

[16] M. A. Addou, J. Lintignat, R. Gomez-Garcia, B. Barelaud, F. Torres, S. Bila, and B. Jarry, "Silicon-integrated signal-interference dual-band bandpass filter for GNSS application," in *IEEE MTT-S Int. Microw. Symp. Dig.*, Honolulu, HI, USA, Jun. 2017, pp. 1675–1678.

[17] J.-S. Hong and M. J. Lancaster, *Microstrip Filters for RF/Microwave Applications*. Hoboken, NJ, USA: Wiley, 2001.

[18] Y. Han, Z. Liu, C. Zhang, C. Mei, Q. Chen, K. Hu, and S. Yuan, "A flexible microstrip low-pass filter design using asymmetric pi-shaped DGS," *IEEE Access*, vol. 7, pp. 49999–50006, 2019.

[19] Y. Liu, L. Liu, C. Liang, and I. Majid, "Compact planar tunable filter with constant absolute bandwidth and wide-frequency tuning range using DGS coupling structure," *IEEE Access*, vol. 9, pp. 157259–157266, 2021.

[20] A. A. Ibrahim, H. A. Mohamed, A. R. D. Rizo, R. Parra-Michel, and H. Aboushady, "Tunable filtenna with DGS loaded resonators for a cognitive radio system based on an SDR transceiver," *IEEE Access*, vol. 10, pp. 32123–32131, 2022.

[21] Y. Rao, H. J. Qian, B. Yang, R. Gomez-Garcia, and X. Luo, "Dual-band bandpass filter and filtering power divider with ultra-wide upper stopband using hybrid microstrip/DGS dual-resonance cells," *IEEE Access*, vol. 8, pp. 23624–23637, 2020.
[22] B. C. Pan, P. Yu, Z. Liao, F. Zhu, and G. Q. Luo, "A compact filtering power divider based on spoof surface plasmon polaritons and substrate integrated waveguide," *IEEE Microw. Wireless Compon. Lett.*, vol. 32, no. 2, pp. 101–104, Feb. 2022.
[23] S. Dey, S. Dey, and S. K. Koul, "Isolation improvement of MIMO antenna using novel EBG and hair-pin shaped DGS at 5G millimeter wave band," *IEEE Access*, vol. 9, pp. 162820–162834, 2021.
[24] D. Gao, Z.-X. Cao, S.-D. Fu, X. Quan, and P. Chen, "A novel slot-array defected ground structure for decoupling microstrip antenna array," *IEEE Trans. Antennas Propag.*, vol. 68, no. 10, pp. 7027–7038, Oct. 2020.
[25] T. Sarkar, A. Ghosh, L. L. K. Singh, S. Chattopadhyay, and C.-Y.-D. Sim, "DGS-integrated air-loaded wideband microstrip antenna for X- and Ku-band," *IEEE Antennas Wireless Propag. Lett.*, vol. 19, no. 1, pp. 114–118, Jan. 2020.
[26] A. Y. I. Ashyap, S. H. B. Dahlan, Z. Z. Abidin, M. H. Dahri, H. A. Majid, M. R. Kamarudin, S. K. Yee, M. H. Jamaluddin, A. Alomainy, and Q. H. Abbasi, "Robust and efficient integrated antenna with EBG-DGS enabled wide bandwidth for wearable medical device applications," *IEEE Access*, vol. 8, pp. 56346–56358, 2020.

XUE MAO received the B.S. degree in communication engineering from Yantai University, Yantai, China, in 2019. She is currently pursuing the M.S. degree with Liaoning Technical University. Her current research interests include communication circuit system design and reconfigurable filter design.

WENJIN LIU received the M.S. degree in computer science and technology from the Liaoning University of Engineering and the Liaoning Technical University, in 2005. She is currently an Associate Professor and a Postgraduate Supervisor with Liaoning Technical University. Her main research interests include image recognition and processing and signal detection and processing.

JINGCHANG NAN received the Ph.D. degree in electromagnetic field and microwave technology from the Beijing University of Posts and Telecommunications, Beijing, China, in 2007. He was a Senior Visiting Scholar at University Michigan, in 2012, ICNC-FSDK2013, and CISP-BMEI2014. He was the Chairperson of the CISP-BMEI2015 Organizing Committee and the Leader of the first-level Discipline of Information and Communication Engineering, Liaoning Technical University. He is currently the Dean, a Professor, and a Doctoral Supervisor with the School of Electronics and Information Engineering, Liaoning Technical University, and a Distinguished Professor of Liaoning Province. His current research interests include RF circuit and systems, electromagnetic field and microwave technology, communication signal processing, and information processing.